



# Treball Final de Grau

Effect of doping on lead-free dielectric ceramics.

Efecte del dopatge en ceràmiques dielèctriques lliures de plom.

Paula Fàbregas Bellavista

*January 2018*





Aquesta obra esta subjecta a la llicència de:  
Reconeixement–NoComercial–SenseObraDerivada



<http://creativecommons.org/licenses/by-nc-nd/3.0/es/>



*"I have not failed. I've just found 10,000 ways that won't work."*

Thomas A. Edison

I would like to thank my degree's final project director Lourdes Mestres for all her patience and for leading me through all this journey of discovery. In particular I am very thankful for her highly accurate professional advice and for sharing with me her passion for knowledge.

A debt of gratitude to my lab mates. I could not have been able to conclude this work without their crucial assistance, their closeness and their understanding. I really enjoyed the time spent in the Solid State Chemistry group as a researcher.



# REPORT





# CONTENTS

<b>1. SUMMARY</b>	3
<b>2. RESUM</b>	5
<b>3. INTRODUCTION</b>	7
3.1. Theoretical concepts	8
3.1.1. Piezoelectricity and ferroelectricity	8
3.1.2. Perovskite structure	10
3.1.3. Piezoelectric lead-free ceramics	11
3.1.4. BNT-BT	13
3.1.4.1. Doping BNT-BT	14
3.2. Characterization techniques	14
3.2.1. X-ray diffraction (XRD)	14
3.2.2. Infrared spectroscopy (IR)	15
3.2.3. Thermal analysis (TGA-DTA)	16
3.2.4. Impedance spectroscopy (IS)	16
3.2.5. Scanning electron microscopy (SEM)-Energy dispersive X-ray spectroscopy (EDS)	17
<b>4. OBJECTIVES</b>	19
<b>5. EXPERIMENTAL SECTION</b>	20
<b>6. RESULTS AND DISCUSSION</b>	27
6.1. X-ray diffraction	27
6.2. Scanning electron microscopy (SEM)-Energy dispersive X-ray spectroscopy (EDS)	30
6.3. Impedance spectroscopy	33
6.4. Ferroelectric properties	35
<b>7. CONCLUSIONS</b>	37
<b>8. REFERENCES AND NOTES</b>	39
<b>9. ACRONYMS</b>	40



# 1. SUMMARY

Piezoelectric materials are widely used nowadays in a large number of electronic devices considering their exceptional electrical properties. Lead zirconate titanate (PZT) is the most currently used piezoelectric material; it presents a perovskite structure and has a region, called morphotropic phase boundary (MPB), where an improvement of its properties occurs. However, the major inconvenience with this material is the environmental and health problems arising from the presence of lead as a result of its high toxicity. For this reason the need for researching on lead-free ceramics with similar properties that PZT shows has been recently one of the main objectives of the scientific community.

$\text{Bi}_{0.5}\text{Na}_{0.5}\text{TiO}_3\text{-BaTiO}_3$  (BNT-BT) system is a promising choice for being the substitute of PZT due to the fact that it has perovskite structure as well as a MPB where great piezoelectric response is obtained. Notwithstanding, even with the large number of studies carried out the exact composition where its properties are as remarkable as the PZT ones has not been found. Consequently, it is necessary to continue investigating in this direction.

This work is based on the study of how the addition of zirconium as a doping element affects BNT-BT properties. The preparation of BNT-BT based ceramics has been made by solid state reaction with variations on the synthesis conditions and composition of the ceramics. Their characterization has been accomplished with the different techniques used on solid state chemistry. Through XRD the introduction of dopants on the BNT-BT structure has been confirmed and by SEM/EDS ceramics could be found where in the structure the dopant goes. Furthermore, the dielectric likewise the ferroelectric properties could have been studied, obtaining different results depending on the synthesis conditions carried through and the composition.

**Keywords:** piezoelectric materials, lead-free, solid state reaction, BNT-BT, doping.



## 2. RESUM

Els materials piezoelèctrics són àmpliament emprats avui en dia en diversos dispositius electrònics degut a les seves excel·lents propietats elèctriques. El titanat zirconat de plom (PZT) és el principal material piezoelèctric; presenta estructura perovskita i té una regió, coneguda com a transició de fase morfoftròpica (MPB), on les seves propietats milloren notablement. Malauradament, aquest material presenta un gran inconvenient i és la presència de plom degut a la seva elevada toxicitat, que resulta ser perjudicial per la salut i el medi ambient. Per aquest motiu, la recerca de ceràmiques lliures de plom amb propietats similars a les del PZT és actualment un dels principals camps d'investigació de la comunitat científica.

Les ceràmiques basades en el  $\text{Bi}_{0.5}\text{Na}_{0.5}\text{TiO}_3\text{-BaTiO}_3$  (BNT-BT) són un bon candidat per substituir el PZT ja que presenta característiques similars a les del PZT, té estructura perovskita així com també una regió de transició de fase morfoftròpica (MPB) on mostra una bona resposta piezoelèctrica. Malgrat la gran quantitat d'estudis que s'han realitzat, no s'ha aconseguit trobar la composició exacta en què les propietats siguin igual de bones que les de PZT. Conseqüentment, és necessari continuar investigant en aquesta direcció.

Aquest treball està basat en l'estudi de com es veuen afectades les propietats del BNT-BT a l'introduir el zirconi com a dopant. La preparació de les ceràmiques basades en el BNT-BT s'ha portat a terme per reacció en estat sòlid amb diverses variacions pel que fa a les condicions de síntesi i també pel que fa a la composició. La caracterització d'aquestes ceràmiques s'ha realitzat segons les diferents tècniques utilitzades en la química de l'estat sòlid. Mitjançant la difracció de raig X s'ha pogut confirmar la introducció del zirconi dins l'estructura i, gràcies a SEM/EDS, s'ha pogut veure on es troba el zirconi. A més a més, les propietats dielèctriques així com les ferroelèctriques s'han pogut estudiar obtenint diferents resultats en funció de les condicions de síntesi emprades i la composició.

**Paraules clau:** material piezoelèctric, lliure de plom, reacció en estat sòlid, BNT-BT, dopatge.



### 3. INTRODUCTION

The discovery of ferroelectricity and piezoelectricity started at 1600 when Elie Seignette prepared for first time a compound, known as La Rochelle salt, which was a sodium potassium tartrate. Although, it was not until 1824, 200 years later, when David Brewster observed the pyroelectricity phenomenon in various crystals, which included La Rochelle salt. However, the first documented works about piezoelectricity were made by Jacques and Pierre Curie in 1880 when they established the direct and inverse piezoelectric effect [1].

In the event of polycrystalline ceramic materials, discovery history of ferroelectricity and piezoelectricity started with the World War II due to the fact those materials created great interest by military applications. One of the further progresses in this field was the breakthrough of solid solutions of lead zirconate titanate by B. Jaffe and collaborator in 1954. Since then, numerous applications have been developed thanks to this discovery and PZT, lead zirconate titanate, has become the most important piezoelectric in the industry [1].

Applications of piezoelectric materials encompass a wide range thanks to its properties. When an alternating voltage is applied, the material oscillates at a specific frequency producing as a result the vibration of a membrane; this fact generates sound and it is used for all type of speakers and headphones. To the contrary, if a mechanical stress is applied, a voltage is generated and then it is used in microphones, lighter flint stones and more. Other uses include radars, computers hard drives and USB memories, sensors, touch screen displays and even injectors of engines.

These ceramics are synthesised by the knowledge provided by solid state chemistry, which is concerned with the synthesis, structure, properties and applications of solid materials. The materials are usually inorganic, but not exclusively so. The products of solid state reactions are usually in the form of a powder or a sintered, polycrystalline piece [2]. The study presented in this work will be focalised on the piezoelectric polycrystalline ceramics, which are ceramics that once poled present piezoelectric properties, its characterization and further study of its properties.

## 3.1. THEORETICAL CONCEPTS

### 3.1.1. Piezoelectricity and ferroelectricity

Piezoelectric materials are those that exhibit the piezoelectric effect, either naturally or when poled. This effect refers to the ability that some materials have to generate an electric potential when a mechanical stress is applied and vice versa.

One characteristic of piezoelectric crystals is that are electrically neutral even though the ions may not be symmetrically arranged, meaning that piezoelectricity is produced in no centrosymmetric structures. When the crystal receives a stress the structure can be deformed generating, as a result, little dipoles, due to the stress applied alters the separation between the positive and negative charged sites in each elementary cell. This polarization, which is direction-dependent (anisotropic), is responsible for generating the electric field, above mentioned, which can be used to transform the mechanical energy into electrical energy.

When the voltage is generated from the application of stress, it is referred to direct effect and the material behaves as a generator or sensor. Instead, when the ceramic is deformed by an applied electric field, it is referred to inverse effect and the material behaves as an actuator.

Besides, all piezoelectric materials are dielectric which means they are all insulators. Inside the piezoelectric pyroelectric materials are classified. These materials when subjected to temperature changes undergo electric polarization variations, in other words, temperature variations induce an electric field originated by the movement of negative and positive charges in the opposite edges of the surface. Inside the pyroelectric group another subgroup exists which is the ferroelectric materials. These materials exhibit spontaneous polarization in the absence of an electric field and this polarization can be switched by applying an electric field. Moreover, when the electric field is removed the field sustains itself. These entire phenomena are related to the crystalline structure of the materials therefore there is a relationship between symmetry and physics external properties.

One distinguished characteristic of these materials is the existence of domains. These domains are crystal sections where each have dipolar moment orientated in the same direction but its neighbours have it in a diverse orientation.

When no polarization is present, the overall polarization is zero, point 1 in Figure 1, due to the fact that domains are in random orientation. However, when electric field is applied all



domains orientate themselves. Furthermore, if electric field intensity is increased, maximum value of polarization can be reached when all domains are oriented to the field direction; this point is known as saturation polarization,  $P_s$ , point 2 in Figure 1.

When the external field is removed, the polarization does not drop to zero and shows remnant polarization, established as  $P_r$ , point 3 in Figure 1. This occurs because the dipoles become less aligned but do not return to the original alignment. When an opposite direction voltage is applied, all domains will orientate to this voltage until all of them get aligned arriving to the saturation polarization point. The coercive field,  $E_c$ , is the electric field needed to apply in order to reduce remnant polarization to zero, point 4 in Figure 1.

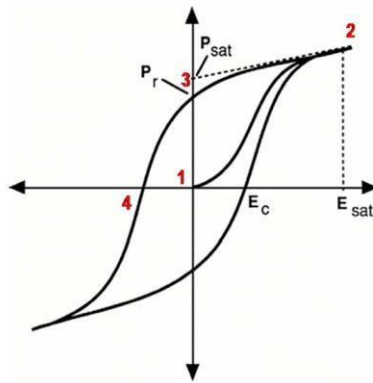


Figure 1. Ferroelectric hysteresis cycle.

(Image obtained from C. Kittel, ref [3])

At low temperatures is where ferroelectricity is usually observed. The temperature in which ferroelectric properties are lost is Curie temperature,  $T_c$ . At this temperature, a structural phase transition takes place and over such temperature ferroelectric phase results in paraelectric phase. At  $T_c$ , ferroelectric materials show high dielectric constant or relative permittivity,  $\epsilon'$ , and this one follows Curie-Weiss equation

$$\text{Equation 1: } \epsilon' = \frac{C}{(T-\theta)}$$

where  $C$  is Curie constant and  $\theta$  is Curie-Weiss temperature. Relative permittivity has usually a maxim value at the temperature where the ferroelectric-paraelectric phase transition occurs.

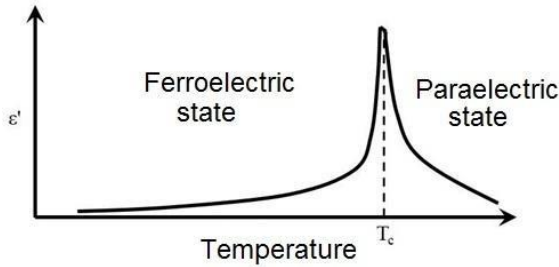


Figure 2. Relative permittivity dependence with temperature of a ferroelectric material

This variation of permittivity in function of the temperature can appear as one of these transitions shown on Figure 3.

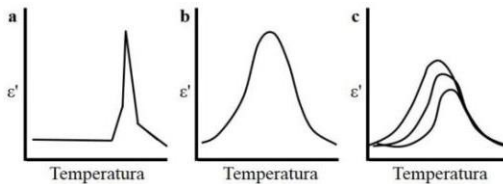


Figure 3. Schematic diagram of dielectric behaviour for barium zirconate titanate. a. Normal, b. Diffuse, c. Relaxor

(Image obtained from W.Li, et al, ref [4])

### 3.1.2. Perovskite structure

Perovskite is a calcium titanium oxide mineral composed of calcium titanate ( $\text{CaTiO}_3$ ). In 1893 Gustav Rose, a German geologist, discovered in the Ural Mountains of Russia this mineral and it was named after Russian mineralogist Lev Perovski (1792–1856) [5].

All the compounds that have the same crystal structure as  $\text{CaTiO}_3$ ,  $\text{ABO}_3$ , are named perovskites. The interest in compounds belonging to this structural family arises from the variety of properties that can show and the flexibility to accommodate a huge part of the elements in the periodic system.

The crystal structure can be described as a net of  $\text{BO}_6$  octahedrons sharing the vertex with other octahedrons and cations A, the bigger ones, occupying the interstitial positions under coordination 12, Figure 4 [5].

Another form to describe it is focusing on cations A, Figure 4(a), which are occupying the centre of the cell and cations B occupying the vertices, the oxygens would be found in the middle of the edges. By focusing on cations B, the structure could be seen as a compact cubic packaging of cations A and oxygen anions, where the cations B occupy the centre of the cell, Figure 4(b). Notwithstanding, this is the quintessential structure and the reality is that perovskite structure materials tend to have distortions which are the responsible for having spontaneous polarizations by reason of the atomic movement of A and B, which results in lower symmetry structures.

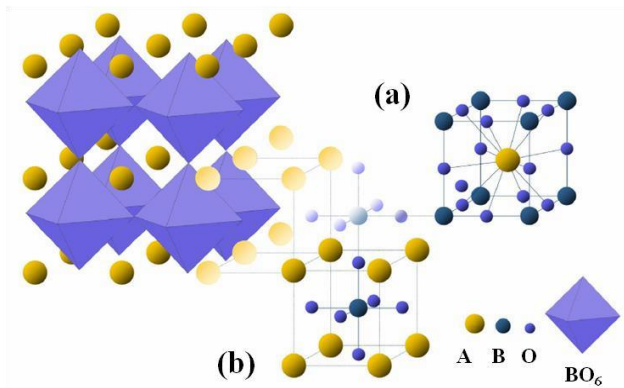


Figure 4. Different representations of the perovskite structure. (a) Cation A centered cell. (b) Cation B centered cell.

This type of crystalline structure is widely studied nowadays. The focus is the study of doping in both positions, A and B, and observing how these changes may influence in properties owned by the material under consideration.

### 3.1.3. Piezoelectric free-lead ceramics

PZT, lead zirconate titanate, which is a solid solution of  $\text{PbZrO}_3$  and  $\text{PbTiO}_3$ , is a ceramic known for having remarkable piezoelectric properties. At certain compositions, this ceramic with a perovskite structure, shows an increase of its properties [6]. These compositions are placed

near a region called morphotropic phase boundary (MPB), and it is a phase transition that occurs at these compositions, around 50%, as shown on Figure 5. It corresponds to the region where a structure change is presented independently of temperature and where tetragonal and rhombohedral structure coexist. Piezoelectric and electromechanical properties of ceramics near the MPB improvement are consequence of higher polarizability, derived from the coexistence of two equivalents energy states. This fact provides a greater and better reorientation of ferroelectric domains during the polarization process. However, PZT is a ruling ceramic in the market not only for its admirable properties, but also because the raw materials needed for its preparation have a low cost.

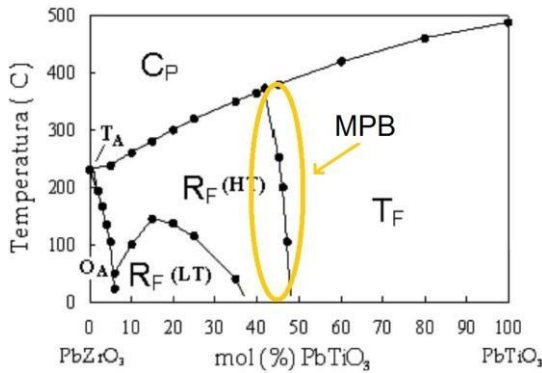


Figure 5. Phase diagram of PbTiO<sub>3</sub>- PbZrO<sub>3</sub> (Cp: cubic-paraelectric phase, R<sub>f</sub> (HT): rhombohedral - ferroelectric phase a high temperatures, R<sub>f</sub> (LT): rhombohedral -ferroelectric phase a low temperatures, OA: orthorhombic-antiferroelectric phase, TF: tetragonal-ferroelectric phase).

(Image based on image from B. Jaffe, et al, ref [6])

The main problem with this compound is the presence of lead since it is qualified as a toxic substance due to its elimination and recycling process can be dangerous for health and environment. For these reasons, the European Union has labelled PZT as a hazardous substance [7], [8].

With that in mind, numerous members of the scientific community are searching nowadays for any substance capable of revealing properties as the PZT ones. One sterling candidate is BNT-BT, which has, as well as PZT has, a MPB where presents a satisfactory piezoelectric behaviour [9], [10]. Moreover, it is an environmentally friendly compound.

### 3.1.4. $\text{Bi}_{0.5}\text{Na}_{0.5}\text{TiO}_3\text{--BaTiO}_3$ (BNT-BT)

Bismuth sodium titanate,  $\text{Bi}_{0.5}\text{Na}_{0.5}\text{TiO}_3$ , BNT, is a piezoelectric material with satisfying properties which makes it, as mentioned above, a solid candidate to substitute PZT in manifold applications. The main similarity is the perovskite structure that both have. Introduction of  $\text{BaTiO}_3$  (BT) improves the properties of BNT and solves the problems that BNT present such as high coercive field,  $E_c$ , which means it is more difficult to polarize, and high conductivity due to bismuth volatilization during the sintering process [11].

The system of  $(1-x)(\text{Bi}_{0.5}\text{Na}_{0.5})\text{TiO}_3 - x\text{BaTiO}_3$ , BNT-BT, has a huge array of compounds depending on the composition ( $x$ ). Around the MPB (near  $x = 0.06$ ) is where the compounds have the best piezoelectric properties. The MPB is formed because in this composition coexist both phases: BNT presents rhombohedral structure at room temperature, and BT presents tetragonal structure.

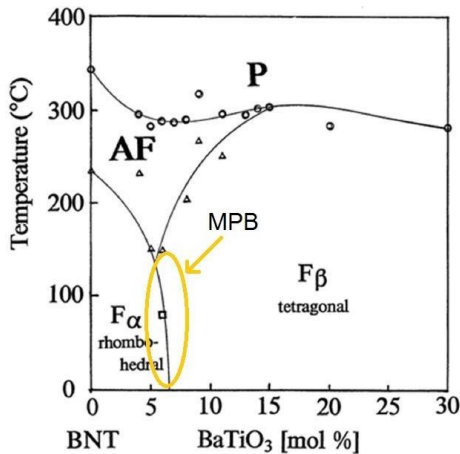


Figure 6. Phase diagram of solid solution of  $(\text{Bi}_{0.5}\text{Na}_{0.5})_{0.96}\text{Ba}_{0.06}\text{TiO}_3$  ( $F_\alpha$ : rhombohedral -ferroelectric,  $F_\beta$ : tetragonal-ferroelectric phase, AF: antiferroelectric phase and P: paraelectric phase).

(Image from T. Takenaka, et al, ref [12])

As it can be seen in Figure 6, BNT-BT shows two phase transitions, one at low temperature which corresponds to ferroelectric - antiferroelectric phase transition and another one at high temperature which is the antiferroelectric - paraelectric phase transition.

Moreover, BNT-BT exhibits a high Curie temperature, which makes the material useful in a wide range of temperatures.

Some drawbacks are the aging effect the material shows and the lack of ability to retain total remnant polarization after being polarized regularly, this effect appears to be dependent on barium titanate content since different values at room temperature are exhibited [11].

#### 3.1.4.1. Doping BNT-BT

BNT-BT is a commendable material that can be utilized in diverse applications considering that its behaviour can be modified. One strategy to modify it is by introducing a dopant agent in its structure; the basis of this method is that these impurities can cause the appearance of disorders, which are the reason why its electrical behaviour can be modified.

In BNT-BT structure two positions can be doped, position A and B. In this essay, position B is the one doped by Zr(IV).

## 3.2. CHARACTERIZATION TECHNIQUES

### 3.2.1. X-ray diffraction (XRD)

It is a technique used to characterize crystalline material, which is the one most used in solid state chemistry. The basis of this technique is in the scattering of the X-ray beam by the periodic structure of the crystal, which has to be seen as a conjunction of crystallographic planes acting as a diffraction lattice. While passing through the sample, the X-ray beam is diffracted by the different planes in many directions. The interference of the diffracted waves gives a pattern of maximums and minimums, called diffraction pattern. When the interaction between the incident rays and the sample creates constructive interference, maximums, Bragg's Law, equation 2, is satisfied. Then the diffracted X-rays are detected and can be processed.

$$\text{Equation 2: } 2d\sin\theta = n\lambda$$

where  $d$  is the distance between plains,  $\lambda$  the wavelength,  $\theta$  the angle and  $n$  a positive integer.

Bragg's Law interprets the crystal to have planes that reflect the X-rays with an angle that equals the incident beam angle, shown in the Figure 7.

The angle is determined by the distance between the different lattice planes; these angles are a fingerprint of the sample considering that each material has a unique fingerprint determined by the present elements and the crystal structure. In addition,  $d$  is related to the cell parameters.

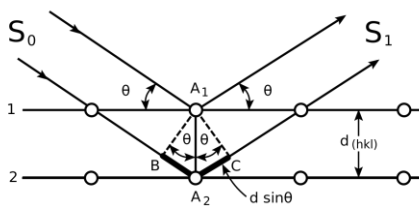


Figure 7. Representation of Bragg's law

(Armicon, 02/12/17 via Wikimedia Commons, Creative Commons Attribution)

X-ray powder diffraction gives information about which phases are present in the sample and allows determining the majority of the crystallographic planes, due to the fact that each plane has its own three Miller indexes,  $hkl$ . This determination is achieved by comparing the diffraction patterns of a sample with the reference one on ICCD [13]. Once the crystallographic planes have been found, the crystallographic parameters of the unit cell ( $a$ ,  $b$ ,  $c$ ,  $\alpha$ ,  $\beta$  and  $\gamma$ ) can be found.

An X-ray powder diffraction pattern is a set of lines or peaks, each of different intensity and position ( $d$ -spacing or Bragg angle,  $\theta$ ). For a given substance, the line positions are essentially fixed and are characteristic of that substance. The intensities may vary somewhat from sample to sample, depending on the method of sample preparation and the instrumental conditions. The more peaks there is in a XRD pattern, the least symmetry the crystal has. Therefore, crystal structures are solved by analyzing the intensities and the peaks of the diffracted X-ray pattern.

XRD characterization was carried out with *PANalyticalX'Pert PRO MDP* diffractometer, with a Ge (111) monochromator. The radiation used was the  $K\alpha$  line of Cu ( $1.5406 \text{ \AA}$ ) at 40 kV and 30 mA, and the diffraction pattern was registered for  $2\theta$  angles from  $10^\circ$  to  $80^\circ$ , with a scanning speed of  $1^\circ/\text{min}$ . The diffraction patterns were studied with the *X'Pert HighScore50* software.

### 3.2.2. Infrared spectroscopy (IR)

This technique is a useful tool for structural determination of the material studying the vibration frequencies of the bonds of the atoms present in the compounds. IR studies the

interaction between matter and IR radiation. The obtained spectrum is generated from the absorption of the photons that have energy corresponding to an IR region, generating a transition between vibrational levels. The absorbed energy, at each wavelength, that can be changed across time can be registered.

The IR measure was made with a *Thermo Nicolet Avatar 330-FT-IR* using frequencies between 400 and 4000  $\text{cm}^{-1}$ . For that process, pellets of the sample were made by mixing powder of the sample and KBr.

### 3.2.3. Thermal analysis (TGA-DTA)

Thermal analysis is the study of the physical and chemical properties of a sample as a function of temperature. The interaction of the sample with heat provides information about chemical and physical processes such as reaction, morphotropic phase changes or physical state changes, and about the intrinsic thermodynamic properties of these processes.

TGA (Thermogravimetric Analysis) is a technique that records the change in weight of a sample as a function of either temperature or time. The information provided is the exact temperature where a process involving a mass change in the sample occurs. When the weight of the sample is represented in front of the temperature, a characteristic curve is obtained. The temperature of the process can be studied from the midpoint of this curve, and find out if the decomposition is complete by comparing the weight loss observed with the theoretical one.

DTA (Differential Thermal Analysis) measures the difference in temperature between a sample and an inert reference material as a function of temperature. The temperature of sample and reference should be the same until some thermal event, such as melting, decomposition or change in crystal structure occurs in the sample, in which case the sample temperature either lags behind or leads the reference temperature. The results obtained allow seeing if it is about an endothermic or exothermic process as well as the reversibility or irreversibility of the process.

Both experiments were done with *Mettler TGA/SDTA 851e/LF/1100* thermobalance in *Serveis Científicotècnic of Universitat Politècnica de Catalunya*

### 3.2.4. Impedance spectroscopy (IS)

Impedance spectroscopy is routinely used to characterize the electrical transport properties of composite electroceramics with heterogeneous microstructures. It studies the properties of



these materials as a function of temperature and frequency, such as relative permittivity (the resistance of the electric field applied) and  $\tan \delta$  (the amount of capacitance lost in form of heat due to crystalline defects). The technique is based on the application of an alternate current in a pellet of the material under consideration, which is placed between two electrodes. Since the surface must be conductive, it is covered by a thin layer of gold by plasma sputtering.

For the reason that it is an alternate current, capacitance measured will have two components, the real part which represents the value of dielectric constant and the imaginary one, which indicates the dielectric losses.

Some considerations for the material being an appropriate material are porosity of the material, due to it must be dense without air inside so all the measures are only for the material and not for air influence, as well as secondary phases, heterogeneities, crystalline defects and grain size because relative permittivity could be influenced by these.

This technique also determines the dielectric anomalies related to phase transitions on the material.

The characterization was carried out with an impedance analyzer HP 4192A from the *Química del Estat Sòlid* group of the *Departament de Química Inorgànica i Orgànica, secció Química Inorgànica* of the *Universitat de Barcelona*.

### **3.2.5. Scanning electron microscopy (SEM) - energy dispersive X-ray spectroscopy (EDS)**

The interaction of electrons with matter is a complex subject of study in which many processes like absorption, emission and reflection are involved. The amount of phenomena indicates that a lot of information can be obtained by irradiating a sample with electrons. Thus, many characterization techniques are based on electron-solid matter interaction. SEM is one of these techniques aforesaid.

This technique studies some of the phenomena that take place when atoms are hit by highly voltage electron beam. These electrons are the secondary electrons, which are emitted from the outer shells of the atoms and have low energy; these ones provide information related to the morphology of the surface and the grain size. There is another type of electrons that can be studied by SEM, these are the backscattered electrons, which are the electrons from the incident beam that suffer dispersion, elastic collision, while they are hitting the atoms under the

surface. The dispersions depend on the weight of the atom, therefore heavier atoms disperse more than the lighter ones and this is used in order to have contrast on the image.

Energy Dispersive Spectroscopy (EDS) allows one to identify particular elements present in the sample and their relative proportions. This technique is based on the ionization phenomenon, which emerges from the interaction between matter and an electron beam. When the sample is beamed with high energy electrons, atoms are ionized and they emit electrons from all the different layers, including the deeper ones. When an electron from valence layer is relaxed, the system emits radiation of a certain wavelength. These X-rays are characteristic from each element.

In order to perform SEM study, the surface of the sample must be conductive. In consequence, the sample was covered by a thin layer of graphite. The study was made on the *Centres Científics i Tecnològics of the Universitat de Barcelona*, with a *JEOL-J-7100-FE* scanning electron microscope in high vacuum conditions and EDS system (Oxford Instruments, INCA).

## 4. OBJECTIVES

The main objective of this work is to evaluate the effect of the synthesis pathway and of doping on the functional properties of BNT-BT based ceramics. In order to accomplish the main objective, concrete objectives must be carried out.

- Optimizing the synthesis conditions.
- Optimizing the sintering conditions to obtain high density ceramics.
- Characterization of the ceramics with the purpose of knowing how zirconium has been introduced in the BNT-BT structure.
- Electric characterization in order to study the dielectric and ferroelectric properties of the ceramics.
- Study the effect of the synthesis conditions on the functional properties of the ceramics.
- Study the effect of varying the amount of zirconium on the electric properties.

## 5. EXPERIMENTAL SECTION

In this project, two different compositions of zirconium doped BNT-BT were studied; the difference was the variation of the amount of Zr added in BNT-BT at the Ti site. The general formula was this one:  $(\text{Bi}_{0.5}\text{Na}_{0.5})_{0.94}\text{Ba}_{0.06}(\text{Ti}_{1-y}\text{Zr}_y)\text{O}_3$   $y = 0.01; 0.03$  (BNT-BTZr $_y$ ). Both compositions were prepared following the solid state reaction procedure and subsequent characterization.

With the purpose to prepare a dense ceramic, and in order to have a reproducible process, all the stages were optimised. The stages required in the solid-state reaction are the following ones: 1. Particle size homogenization, 2. Thermal treatment, 3. Mixture and homogenization, 4. Calcination, 5. Grinding, 6. Sintering. To obtain the doped compounds of BNT-BT the following raw materials are the ones needed, Table 1.

Raw material	Sigma- Aldrich reference CAS	Purity [%]	Molecular Weight [g/mol]	Powder colour
$\text{Bi}_2\text{O}_3$	1304-76-3	99.9	465.96	Yellow
$\text{Na}_2\text{CO}_3$	497-19-8	99.5	105.99	White
$\text{BaCO}_3$	513-77-9	99	197.34	White
$\text{TiO}_2$	1317-70-0	99.9	79.90	White
$\text{ZrO}_2$	3141-23-4	99.9	123.223	White

Table 1. Raw materials used in the synthesis of BNT-BTZr $_y$  compounds.

The particle size is another fact that has to be considered, this is because the particle size of all the reagents can influence the synthesis process as well as its properties. For this reason, a proper process with the aim to obtain a similar particle size has to be done. The different reagents have to have, ideally, a small homogenised size to favour the diffusion process that takes places in the solid state reaction [14]. Hence, the size of reagents particles was

determined [15], and it could be established that sodium carbonate has higher particle size on average and broader distribution. In consequence, milling with the planetary ball mill was the previous stage for sodium carbonate.

Once the particle size has been homogenized, the reagents must be treated thermally. Each has to be treated differently from the other ones. On the one hand, sodium and barium carbonates are dehydrated at 200 °C in the furnace during one night. On the other hand, titanium oxide and zirconium oxide are treated at 900 °C and bismuth oxide at 500 °C during 8 hours in order to decarbonatate them. Titanium oxide is fast cooled in order to obtain anatase structure.

After these thermal treatments, carbonates and titanium, zirconium and bismuth oxides are weighted according to the stoichiometry of each composition. Weighted stage is the most important due to the synthesis route is through solid state reaction which means the reagents must be in stoichiometric proportion in order to obtain the specific composition. The mixture of the reagents is milled in a planetary ball mill during 8 hours at 300 rpm, using Y<sub>2</sub>O<sub>3</sub> stabilized ZrO<sub>2</sub> balls of  $\varnothing = 1$  mm and absolute ethanol. Once milled, the balls are separated from the reagents mixture and scattered through ULTRA- TURAX disperser in order to break lumps that might be formed. After the mixture is dried in a hot plate until ethanol evaporates and then, to obtain the dried product, it is left 12 hours at 100 °C to ensure the entire evaporation.

Finally, a stage of sieving with a 90  $\mu$ m stainless steel sieve mesh is done to obtain small and homogeneous particle size and make it easier for the reaction to take place.

### **Calcination**

Thermal analysis allows an establishment of the calcination temperature by virtue of this analysis provides knowledge about the behaviour of the reagents mixture in front of the temperature. The results are shown in the Figure 8. The interval studied is between 25 °C and 1000°C; in this interval the sample shows a global mass loss of ~ 10%. In order to clarify concretely the temperature, which each associated phenomenon takes place, a derivate of the thermogravimetric analysis has been illustrated. As it can be seen there are three weight loses, such loses are associated to endothermic reactions, which take place at 90 °C, 390 °C and 600 °C as it can be seen with DTA.

At low temperatures, the peak at 90°C is the one found; the loss appreciated is attributed to water elimination. Continuing with the increase of temperature, the next peak observed is the

one at 390 °C, which jointly with the peak at 600 °C, is associated with the weight loss of CO<sub>2</sub> resulting from the carbonates present in the reagents mixture.

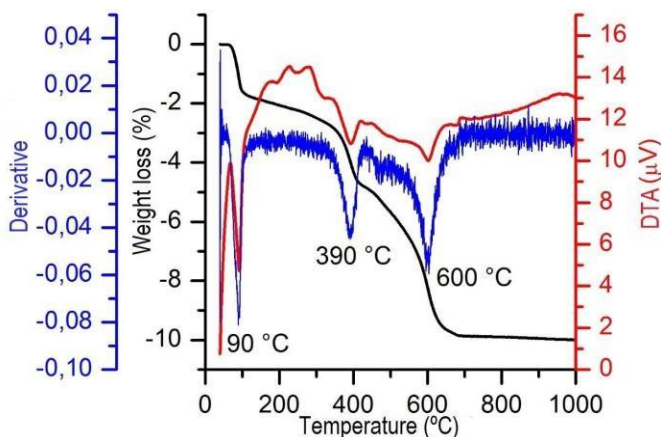


Figure 8. Thermogravimetric analysis for BNT-BT

Therefore, bearing in mind the molecular weight of each reagent and all the products obtained, the weight lost can be estimated during the reaction where the bismuth and sodium titanate-barium titanate is formed. Then, the loss of the CO<sub>2</sub> is consistent with the obtained value by thermogravimetric analysis.

The decomposition of carbonates and the formation of BNT-BT perovskite are completed when the temperature arrives at 700 °C due to the fact that over this temperature any weight loss can be seen and neither a change in the DTA can be observed. In order to study the perovskite's formation process as well as the optimum synthesis temperature and with the information that these results provide, different temperatures were selected to make a thermal treatment during 2 hours, Figure 9.

The reagents mixture was thermally treated over 300 °C, temperature which the carbonates decomposition begins, concretely at 500 °C, when decomposition is not yet complete; also at 700 °C, temperature from which carbonates should have been decomposed completely and perovskite should have been formed agreeing with the thermal analysis. The third temperature was 800 °C due to Zr is heavier than Ti and it might need more temperature to form perovskite structure.

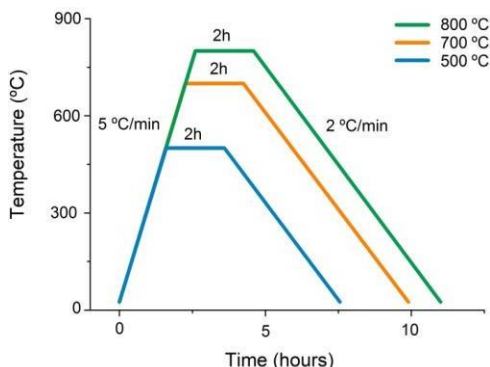


Figure 9. Calcination profiles and temperatures selected

Moreover, to complement this study powder from BNT-BT calcined at different temperatures were characterised by IR and XRD.

The IR spectrum, Figure 10, shows three distinguished bands at  $\sim 1450\text{ cm}^{-1}$ , at  $\sim 800\text{ cm}^{-1}$  and at  $\sim 630\text{ cm}^{-1}$ .

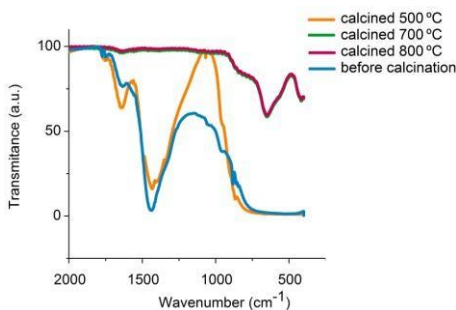


Figure 10. Comparison of IR spectra obtained from the powder calcined at different temperatures

The band situated at  $1450\text{ cm}^{-1}$  is assigned to the asymmetric tension from C-O ( $\nu_3$ ), typical from carbonates. The band at  $800\text{ cm}^{-1}$  is associated with the deformation vibration out of the plane ( $\nu_2$ ) of the carbonate. The one at  $630\text{ cm}^{-1}$  is the one formed from the presence of Ti-O bonds [16].

As it can be observed in the Figure 10, the band at  $1450\text{ cm}^{-1}$ , decreases while the temperature increases until temperature reaches  $700\text{ °C}$ . The result is in concordance with the other results obtained with TGA-DTA, which show that over  $600\text{ °C}$  no weight loss resulting from carbonates are found. If the section of lower length numbers is studied in detail, small variations

can be observed depending on the thermal treatment applied. Focusing on the 500 °C calcination, a wide band is obtained between 900 and 400  $\text{cm}^{-1}$ , whereas a higher temperatures, it gets thinner significantly. By this fact, it can be deduced that, at temperatures above 500 °C the carbonate band disappears and gives way to a thinner band related to the characteristic vibration of  $\text{TiO}_6$  octahedrons, which can be assigned to Ti-O vibrations. The happening of this band confirms that perovskite structure is formed at 700 °C [17].

X-ray diffraction pattern set the calcined samples at different temperatures out in Figure 11.

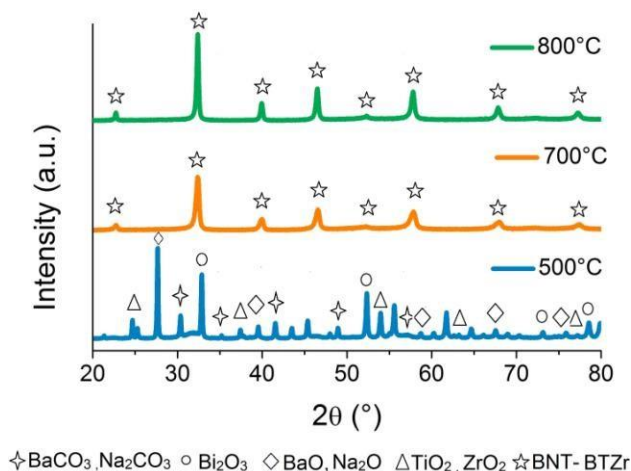


Figure 11. XRD patterns of BNT-BTZr0.01 calcined powder at different temperatures

At 500 °C, the X-ray pattern shows maximums which are related to barium oxide and sodium oxide. According to thermogravimetric analysis, aforementioned, the reaction has begun and new products, which are obviously the ones produced in carbonates decomposition, appear. Even so, there are some peaks that could not be assigned and thereupon it can be an intermediate phase.

Conversely, when treated at 700 °C, a unique phase can be appreciated. The phase aforesaid, is assigned to bismuth and sodium titanate – barium titanate perovskite. These results concur with the ones attained on both thermogravimetric analyses as well as on infrared spectroscopy. At 800 °C the peaks, although they are the same ones of the XRD obtained at 700 °C, appear more intensive and narrower which suggest it is a more crystalline powder. Ergo, 800 °C is established as the optimal calcination temperature for these ceramics.



### **Calcined powder grinding**

Eventually, after the calcination process, obtained powder is grinded again with the purpose of reducing the particle size of zirconium doped BNT-BT samples. This stage is performed with a planetary ball mill during 8 hours,  $Y_2O_3$  stabilized  $ZrO_2$  balls of  $\varnothing = 1$  mm in ethanol were used. Once milled, powder mixture and ethanol were separated from balls and an organic additive was added as agglomerate in order to make the following stages, pressing and sintering, easier. The additive chosen was PARALOID-67 (Rohm and Haas), an acrylic polymer. The addition of agglomerate avoids the formation of interior fissure in the pellet while applying high pressures.

The agglomerate was first dissolved in acetone 20 % in weight and a 7 % in weight of calcined powder mixture was added. Finally, the mixture was scattered by ULTRA-TURAX disperser in order to break all the possible agglomerates that might have been formed during the grinding stage.

After this stage, drying and sieving are the next steps. The sieving step was done with a 90  $\mu m$  stainless steel sieve mesh.

### **Sintering**

With the purpose of obtaining dense ceramics a stage of sintering is needed. Therefore, calcined powder were pressed by uniaxial pressing, with pellet form of  $\varnothing = 6$  mm in a hydraulic press applying 700 MPa of pressure.

Compacted samples were sintered at air atmosphere. A decision of making diverse thermal treatments between 1100 °C and 1250 °C during 2 hours was made in order to study the variance of its density. Figure 12 reveals the sintered profiles performed.

The procedure carried trough was the same for all the cases; the sample was deposited over a platinum sheet, recoat with same composition powder and covered with another platinum sheet with the purpose of avoid elements' possible volatilization.

Because of agglomerate was previously added, a treatment at 700 °C for 2 hours, at low heating velocity, is fundamental to be done for the purpose of removing the polymeric additive.

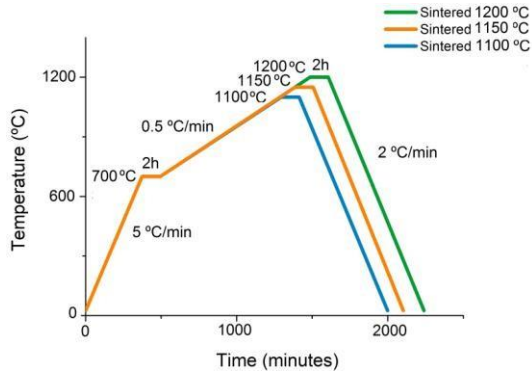


Figure 12. Sintering profiles of the BNT-BTZr

Density was then analysed by two different measurements after thermal treatments of sintering at different temperatures were done. The first one was with a digital calliper and the other one by Archimedes method with the help of the analytical balance with the densities measurement set. In order to obtain the % of relative density, the theoretical density has to be found; this value is obtained by XRD patterns by considering the parameters of the unit cell [2].

Composition	Density [%] on Archimedes method		
	1100 °C	1150°C	1200°C
BNT-BTZr 0.01 calcined 700 °C	90	92	93
BNT-BTZr 0.01 calcined 800 °C	94	95	97
BNT-BTZr 0.03 calcined 800 °C	91	97	97

Table 2. Densities obtained for the sintered pellets at 1100 °C, 1150 °C and 1200 °C.

The results obtained with the digital calliper are of the same magnitude of the ones displayed on Table 2.

As it can be seen, doped BNT-BT's density increases as well as temperature do until it reaches a maximum at 1200 °C. Thus, bearing these results in mind, 1200 °C is established as optimum temperature for ceramics present in this project.

## 6. RESULTS AND DISCUSSION

In order to characterise the different doped BNT-BT based ceramics, each composition was characterised by different techniques: XRD, SEM/EDS and the electric properties were studied.

### 6.1. X-ray diffraction

In terms of XRD, these studies provide information about the crystalline structure. In order to know all this information, a comparison between the experimental patterns and patterns of the powder diffraction file (PDF) was made [13]. The patterns used in the interest of identification the symmetry are the rhombohedral one of BNT (PDF#00-036-0153), the tetragonal of BT (PDF#01-079-2264) and the cubic of BNT (PDF#01-089-3109).

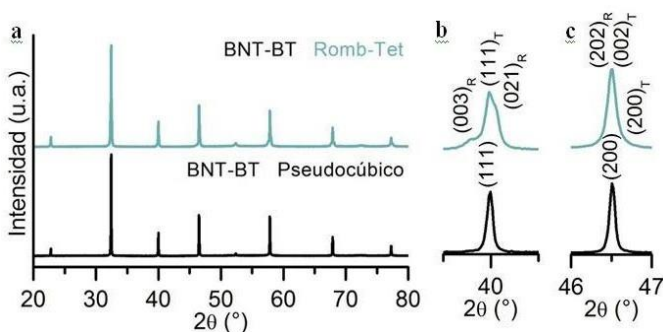


Figure 13. XRD study of undoped BNT-BT

(Image from E. Cerdeiras, ref [15])

The results can show different possibilities. One option is to have coexistence between the tetragonal and the rhombohedral symmetries, Figure 13a blue pattern. The other option is to have a pseudocubic symmetry, Figure 13a black pattern. In order to know if coexistence is present, peaks near  $40^\circ$  and  $46^\circ$  are the ones zoomed because they provide the information needed, the peaks appear with more than one maximum of diffraction and are non-symmetric. As it can be seen in Figure 13b, near  $40^\circ$  rhombohedral symmetry pattern shows two peaks

(03) and (021) while tetragonal pattern only one (111). Studying the  $46^\circ$  region, Figure 13c, rhombohedral pattern shows one peak (202) whereas tetragonal two, (200) and (202). However, when having pseudocubic symmetry these regions of  $40^\circ$  and  $46^\circ$  have only one maximum of diffraction and the peaks are symmetric.

The results shown in Figure 14 are the ones obtained by the BNT-BTZr0.01 calcined at  $800^\circ\text{C}$ . As it can be seen, in all the cases a unique phase of perovskite is observed, Figure 14a).

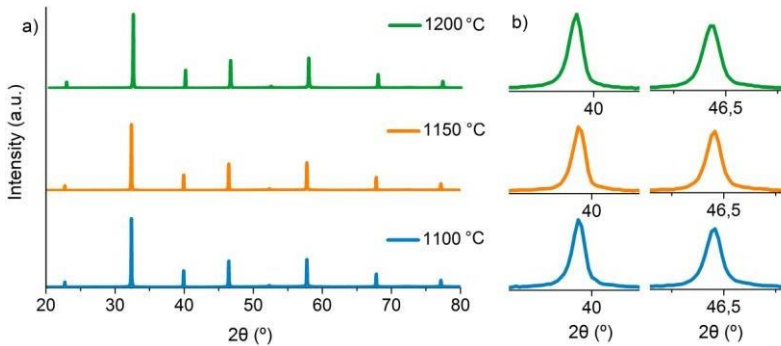


Figure 14. a) XRD study of BNT-BTZr0.01 calcined at  $800^\circ\text{C}$  and sintered at different temperatures; b) zoomed regions of  $40^\circ$  and  $46^\circ$  ( $2\theta$ ).

A detailed exam of the results in the region of  $40^\circ$  and  $46^\circ$ ,  $2\theta$ , shows a unique maximum of diffraction in both regions, Figure 14b. Consequently, the X-ray diffraction patterns of doped ceramics with zirconium indicate the formation of a crystalline phase with pseudocubic symmetry. The same conclusions can be deduced from the results obtained from the diffraction pattern of BNT-BTZr0.01 calcined at  $700^\circ\text{C}$ , Figure 15.

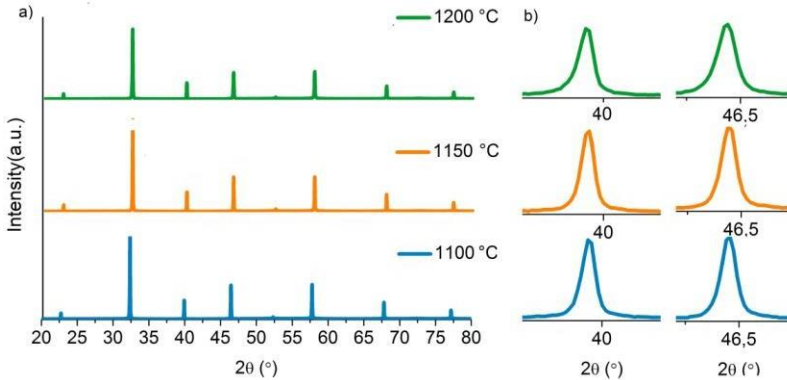


Figure 15. XRD study of BNT-BTZr0.01 calcined at 700 °C and sintered at different temperatures.

The results from the composition BNT-BTZr0.03 are the following ones. On Figure 16 also a unique phase of perovskite is observed. It can also be seen that the peaks are symmetric, which means the pseudocubic symmetry is the one obtained.

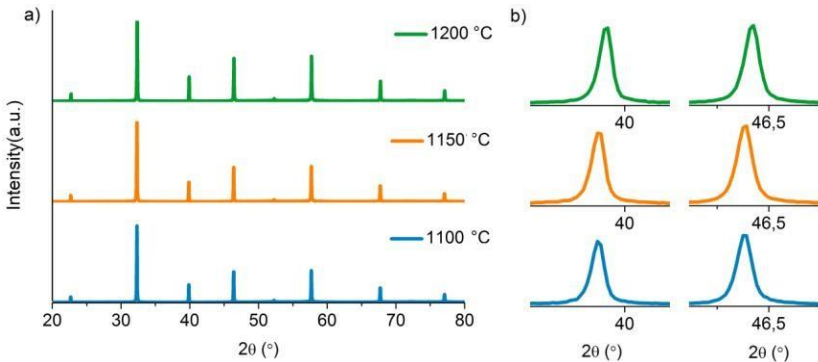


Figure 16. XRD study of BNT-BTZr0.03 sintered at different temperatures

When comparing carefully the XRD patterns from the BNT-BTZry of different compositions a slight displacement of the diffraction maximums to lower angles ( $2\theta$ ) can be highlighted. This fact is visible when zooming the region 40° and 46°, then the differences can be clearly seen compared to BNT-BT, Figure 17. This fact is expected since titanium is the one substituted in the structure for zirconium and the ionic radius of Zr(IV) coordination 6 ( $0.72 \text{ \AA}$ ) is bigger than the ionic radius of Ti(IV) coordination 6 ( $0.605 \text{ \AA}$ ) [18].

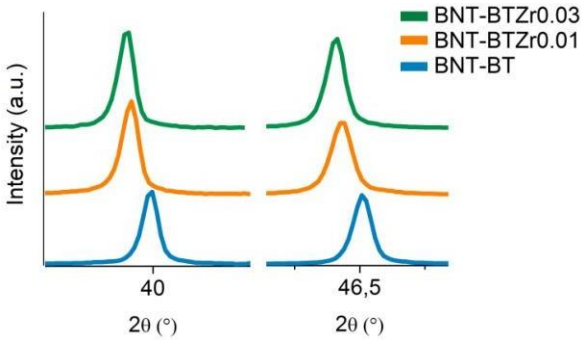


Figure 17. Comparison of the region 40° and 46° of both compositions of BNT-BTZr<sub>y</sub> and BNT-BT

When introducing Zr(IV) in the position B of the perovskite, an increase of the cell volume is also expected. If zirconium is placed in the structure in substitution of titanium in B position of the perovskite, the volume of the unit cell increases as more zirconium is added in the BNT-BT. Figure 18 shows how the volume increases as more zirconium is added. This fact allow assuming that zirconium goes inside the BNT-BT structure.

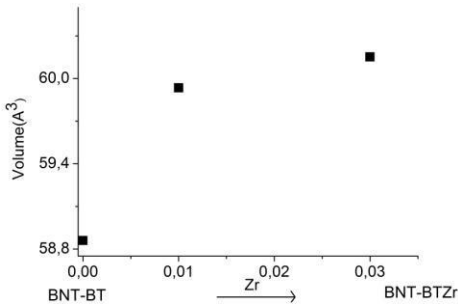


Figure 18. Variation of the cell volume depending on the amount of zirconium added in BNT-BT.

## 6.2. Scanning electron microscopy (SEM) - Energy dispersive X-ray spectroscopy (EDS)

For the analysis of the surface by SEM, all the image were taken at 3000 magnifications. The Scanning electron microscopy micrographs of the BNT-BTZr<sub>0.01</sub> calcined at different temperatures are shown in Figure 19. The images show polycrystalline structure of the ceramics with a compact microstructure. Huge differences cannot be noticed when observing the following images, notwithstanding, when measuring the grain size a variation can be found when varying the calcination temperature, Table 3.

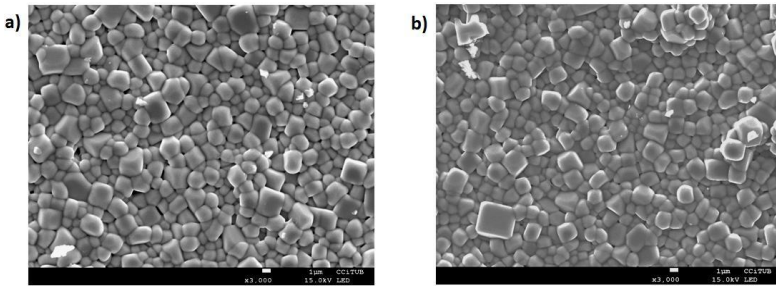


Figure 19. SEM images corresponding to BNT-BTZr<sub>0.01</sub> calcined at different temperatures: a) calcined 700 °C b) calcined 800 °C.

The SEM micrographs of the BNT-BTZr<sub>0.01</sub> calcined at 800 °C and sintered at different temperatures are displayed in Figure 20, being temperatures 1100 °C, 1150 °C and 1200 °C. An increase on the grain size is related to higher sintering temperature. It can be also appreciated the variation of the form of the grains, the ones sintered at 1150 °C have polyhedral shaped grains whereas the other two, the ones sintered at 1100 °C and 1200 °C seem to have rounded contours.

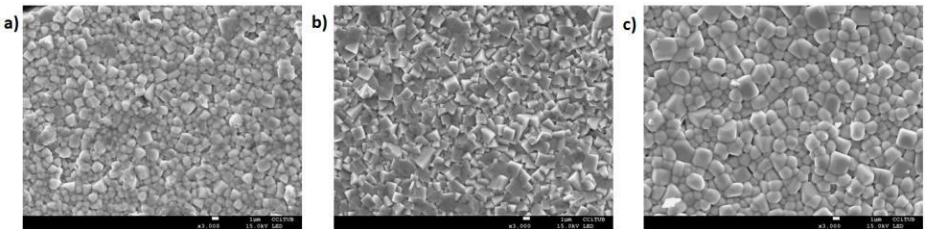


Figure 20. SEM images corresponding to the BNT-BTZr<sub>0.01</sub> sintered at a) 1100 °C, b) 1150 °C and c) 1200 °C.

The analysis of the surface of the BNT-BTZr<sub>y</sub> ceramics by SEM reveal the existence of two evident regions that present different morphology. For this reason different images were taken, one with secondary electrons (SE), Figure 21a), and the other one with backscattered electrons (BSE), Figure 21b), since the different tonality of each region confirms that the region with different morphology have also different composition. With the purpose of knowing the exact composition of each region, a analysis by EDS was performed, Figure 21c) and Figure 21d).

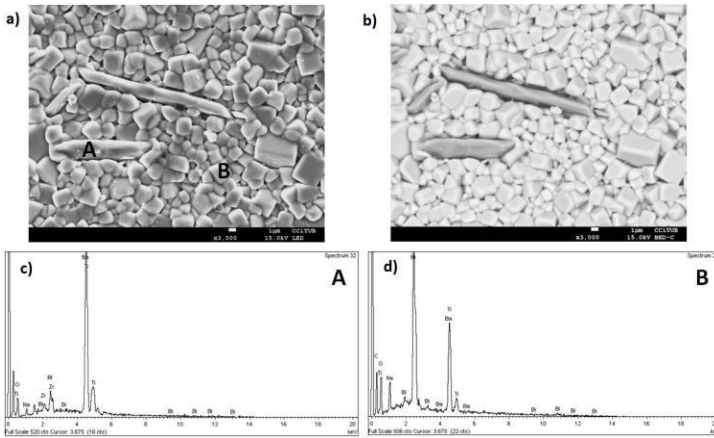


Figure 21. a) SEI and, b) BSE images of BNT-BTZr<sub>0.03</sub> sintered at 1200°C. EDS analysis for A zone c) and B zone d).

The analysis reveals different composition as function of the zone chosen. The region A formed by barium, titanium and zirconium and the brightest region, region B, formed by bismuth, sodium and titanium. Therefore, it can be considered that BNT-BTZr ceramics are formed by a matrix of BNT with grains of BT. Furthermore, it can be established that the dopant is founded in zone A, which means that substitutes the titanium in the BT.

Grain size of the prepared ceramics was analysed by Fullman intersection method [19]. A minimum of 300 grains per image was used on the analysis. The results are shown on Table 3.

Composition	$d_{50}$ ( $\mu\text{m}$ )
BNT-BTZr <sub>0.01</sub> calcined 700°C sintered 1200°C	$1.58 \pm 0.11$
BNT-BTZr <sub>0.01</sub> calcined 800°C sintered 1100°C	$1.25 \pm 0.15$
BNT-BTZr <sub>0.01</sub> calcined 800°C sintered 1150°C	$1.43 \pm 0.17$
BNT-BTZr <sub>0.01</sub> calcined 800°C sintered 1200°C	$1.74 \pm 0.12$

Table 3. Grain size of BNT-BTZr<sub>y</sub> ceramics.

Higher calcination as well as sintering temperature produces an increase of the grain size, as it can be observed, Table 3.



### 6.3. Impedance spectroscopy (IS)

For studying the characteristics of the phase transitions of zirconium doped BNT-BT the relative permittivity as a function of temperature at different frequencies was measured. The results of BNT-BTZr0.01 calcined at 800 °C are shown, Figure 22.

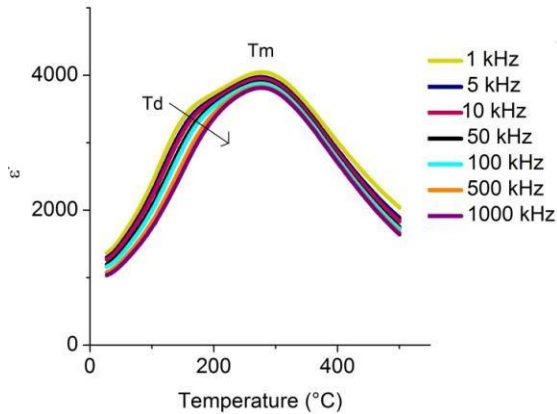


Figure 22. Dependency of the relative permittivity with temperature at different frequencies for BNT-BTZr0.01

The results of the variation of the relative permittivity with temperature reveal the two characteristic dielectric anomalies of the system BNT-BT. The first one, known as the depolarization temperature ( $T_d$ ), is attributed to the ferroelectric-antiferroelectric transition whereas the second one, which is the maximum of permittivity, is related to the antiferroelectric-paraelectric transition ( $T_m$ ). This second point is associated with Curie temperature ( $T_c$ ).

Furthermore, the results reflect clearly how relative permittivity is dependent of frequency near the  $T_d$ . This behaviour is associated with a relaxor phase transition. Whilst the antiferroelectric-paraelectric transition ( $T_m$ ) is wide and independent of frequency, behaviour related to diffuse phase transition.

Figure 23 shows the relative permittivity at 5 kHz in front of temperature of BNT-BT and BNT-BTZr0.01 sintered at different temperatures. Results reveal an increase in relative permittivity with the sintering temperature, the maximum appears at 1200 °C, hence being the optimal sintering temperature for BNT-BT doped with zirconium ceramics. Moreover, in all cases the ceramics display the same behaviour as BNT-BT since all have two dielectric anomalies.

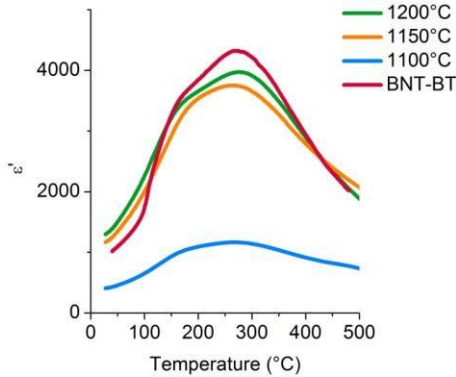


Figure 23. Relative permittivity dependence with temperature for BNT-BTZr0.01 ceramics sintered at different temperatures.

Once 1200 °C was established as the temperature in which BNT-BTZr0.01 reveals the best response of relative permittivity in front of temperature, the study of the effect of the composition was performed between the ceramics of BNT-BTZry sintered at 1200 °C and BNT-BT, Figure 24. The results display that the amount of zirconium modifies the temperatures where the dielectric anomalies take place. The ferroelectric-antiferroelectric transition of BNT-BTZry occurs at lower temperature than the BNT-BT one unlike the antiferroelectric-paraelectric transition of BNT-BTZry which occurs at higher temperature when comparing to BNT-BT, Figure 24a. Ergo,  $T_c$  increases when BNT-BT is doped with zirconium. Moreover, the relative permittivity also decreases when BNT-BT is doped with zirconium.

In the comparative study of dielectric losses evolution with temperature, Figure 24.b, BNT-BTZry present low dielectric losses values while increasing the temperature unlike BNT-BT, which has low dielectric losses since the temperature near  $T_m$ , where the dielectric losses increases slightly. Besides, in all the temperature range, BNT-BTZry has lower dielectric losses than the BNT-BT without doping.

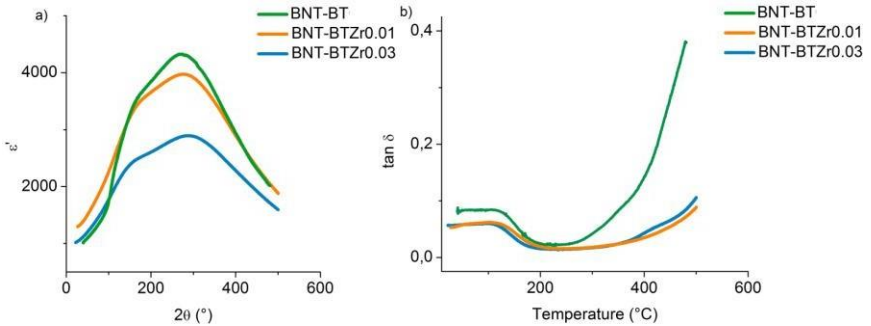


Figure 24. a) Comparison of relative permittivity at 5 kHz between BNT-BT and BNT-BTZry sintered at 1200°C. b) Comparison of dielectric losses between BNT-BT and BNT-BTZry sintered at 1200°C.

#### 6.4. Ferroelectric properties

Figure 25 displays the hysteresis cycle of the ceramic materials based on BNT-BTZry, obtained at room temperature and at 6 kV as well as the BNT-BT. As it can be observed, the addition of zirconium in BNT-BT causes a shortfall of the coercive field,  $E_c$ . Talking about the remnant polarization,  $P_r$ , a decrease can be observed when comparing both compositions of BNT-BTZry although the BNT-BTZr0.01 is similar to the one of BNT-BT.

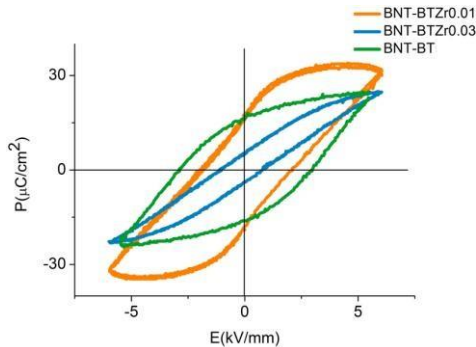


Figure 25. Comparison between BNT-BTZry and BNT-BT hysteresis cycle

Another noticeable difference is the saturation polarizations which are significantly distant between both compositions of BNT-BTZry, although the BNT-BTZr0.03 is similar to the one for BNT-BT. The one with higher remnant polarization is BNT-BTZr0.01, Figure 25.

The sintering temperatures can vary the electric properties such as hysteresis cycle as shown in Figure 26.

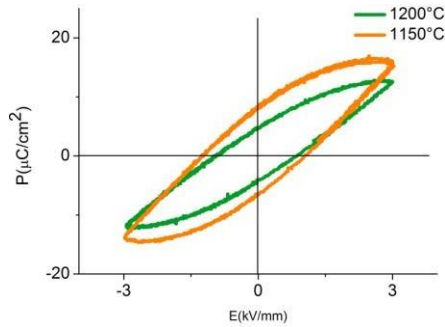


Figure 26. Comparison of hysteresis cycles of BNT-BTZr0.01 pellets sintered at different temperature.

The pellets sintered at lower temperature appear as the ones that have higher coercive field, higher remnant polarization as well as saturation polarization. Furthermore, the ceramic of BNT-BTZr0.03 sintered at 1200 °C was brought up to the limit, and it was found that it could withstand a field of 9 kV as shown in Figure 27. The hysteresis cycle appears as a pinched one.

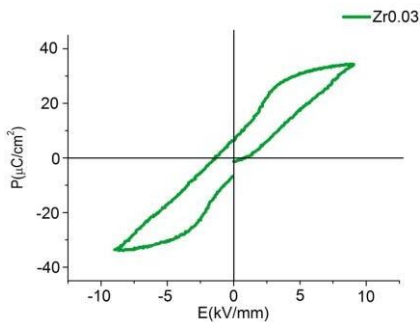


Figure 27. Hysteresis cycle of BNT-BTZr0.03 at 9kV.

## 7. CONCLUSIONS

The main objective was to evaluate how the synthesis pathway and doping modify the functional properties of BNT-BT based ceramics. After this essay has been completed, the following conclusions can be reached.

The optimal conditions in order to obtain high density ceramics based on BNT-BT doped with zirconium are 800°C as calcination temperature and 1200°C as sintering temperature.

BNT-BTZr<sub>y</sub> ceramics with perovskite structure are formed by a matrix of BNT with grains of BT and it is in these grains where zirconium is found.

Electric properties are modified by the sintering conditions. The ceramics sintered at higher temperature present higher relative permittivity, and the ceramics sintered at 1150°C present higher values of  $E_c$ ,  $P_{sat}$  and  $P_r$  than the ceramics sintered at other temperatures.

By doping BNT-BT with zirconium, even though BNT-BTZr<sub>y</sub> ceramics present the two characteristic dielectric anomalies of BNT-BT, phase transition temperatures are modified; the ferroelectric-antiferroelectric phase transition occurs at lower temperature and the antiferroelectric-paraelectric at higher temperature. Furthermore, higher relative permittivity is reached at room temperature, and lower relative permittivity at higher temperature. Moreover, dielectric losses of BNT-BTZr<sub>y</sub> are low, which means a greater behaviour as a dielectric material. Also the values of  $E_c$ ,  $P_{sat}$  and  $P_r$  vary. For these facts it can be assumed that doping affects the dielectric and ferroelectric properties.

The results obtained in this study are conclusive that the synthesis conditions as well as doping allow the modulation of the properties of the BNT-BT based ceramics.



## 8. REFERENCES AND NOTES

1. K. Uchino. *Advanced Piezoelectric Materials: Science and Technology*, 2nd ed, Woodhead Publishing, Jun 2017, 1-5, 95-97.
2. A.R. West. *Solid state chemistry and its applications*, John Wiley & Sons, 1984.
3. C. Kittel. *Introducción a la física del estado sólido*, 3a ed, Ed. Reverté S.A., Barcelona, 1997.
4. W. Li, D. Su, J. Zhu, and Y. Wang. Mechanical and dielectric relaxation in neodymium-modified bismuth titanate ceramics, *Solid State Commun.*, 2014, 131(3-4), 189-193.
5. M.R. Levy. *Crystal structure and defect property predictions in ceramic materials*, University of London, 2005, Chapter 3.
6. B. Jaffe, W.R. Cook Jr., and H. Jaffe. *Piezoelectric ceramics*, Academic Press: London, New York, 1971.
7. EU- Directive 2002/95/EC: Restriction of the use of certain hazardous substances in electrical and electronic equipment (RoHS), *Off. J. Eur. Union*, 2003, 46(L37), 19.
8. EU- Directive 2002/96/EC: Waste electrical and electronic equipment (WEEE). *Off. J. Eur. Union*, 2003, 46(L37), 24.
9. M. Rawat, K. L. Yadav. Structural, Dielectric and Ferroelectric Properties of  $Ba_{1-x}(Bi_{0.5}Na_{0.5})_xTiO_3$  Ceramics, *Ceramics International*, 2012, 39(4), 3627-3633.
10. A. Maqbool, J. Rahman, Ali. Hussain. Structure and temperature dependent electrical properties of lead-free  $Bi_{0.5}Na_{0.5}TiO_3$ - $SrZrO_3$  ceramics, *IOP Conf. Ser.: Mater. Sci. Eng.*, 2014, 60, 1-3.
11. B. Parija, T. Badapanda, S. Panigrahi, T.P. Sinha. Ferroelectric and piezoelectric properties  $(1-x)(Bi_{0.5}Na_{0.5})TiO_3$ - $xBaTiO_3$ , *J. Mater Sci.: Mater Electron*, 2013, 24, 402-410.
12. T. Takenaka, K. Maruyama, and K. Sakata.  $(Bi_{1/2}Na_{1/2})TiO_3$ - $BaTiO_3$  System for Lead-Free Piezoelectric Ceramics, *Jpn, J. Appl. Phys.*, 1991, 30, 2236-2239.
13. International center for diffraction data (ICDD).
14. H. D. Megaw. *Crystal structures, a working approach*, 10th ed, Ed. Saunders, 1973.
15. E. Cerdeiras. *Materiales piezoeléctricos derivados del  $(Bi_{0.5}Na_{0.5})TiO_3$ - $BaTiO_3$ : preparación y estudio de las propiedades funcionales*, 2016.
16. K. Nakamoto. *Infrared and Raman Spectra of Inorganic and Coordination Compounds*, 6th ed, John Wiley & Sons, New Jersey, 2009.
17. R.S. Puche and P. Caro. *Rare Earths*, Ed. Complutense, S.A., Madrid, 1998.
18. R. D. Shannon. Revised Effective Ionic Radii and Systematic Studies of Interatomic Distances in Halides and Chalcogenides. *Acta Crystallogr., Sect. A*, 1976, 32(5), 751-767.
19. J.W. Cahn and R. L. Fullman. On the Use of Linear Analysis for Obtaining Particle Size Distribution Functions in Opaque Samples, *J. Met.*, 1956, 8, 610.
20. Jones G.O., Thomas P.A. Investigation of the structure and phase transitions in the novel A-site substituted distorted perovskite compound  $Na_{0.5}Bi_{0.5}TiO_3$ . *Acta Crystallogr. Sect. B Struct. Sci.*, 2002, 58(2), 168-78.
21. G. Picht, J. Töpfer, E. Hennig. Structural properties of  $(Bi_{0.5}Na_{0.5})_{1-x}BaxTiO_3$  lead-free piezoelectric ceramics, *J Eur. Ceram. Soc.*, 2010, 30(16), 3445-53.

## 9. ACRONYMS

BNT-BT:  $(\text{Bi}_{0.5}\text{Na}_{0.5})\text{TiO}_3$  -  $\text{BaTiO}_3$

BNT-BTZry:  $(\text{Bi}_{0.5}\text{Na}_{0.5})_{0.94}\text{Ba}_{0.06}(\text{Ti}_{1-y}\text{Zr}_y)\text{O}_3$

XRD: X-ray diffraction

IS: Impedance spectroscopy

SEM: Scanning electron microscopy

EDS: Energy dispersive X-ray spectroscopy

MPB: Morphotropic phase boundary



